

A Novel Framework for Cellular Tracking and Mitosis Detection in Dense Phase Contrast Microscopy Images

Ketheesan Thirusittampalam, M. Julius Hossain, *Member, IEEE*, Ovidiu Ghita, and Paul F. Whelan, *Senior Member, IEEE*

Abstract—The aim of this paper is to detail the development of a novel tracking framework that is able to extract the cell motility indicators and to determine the cellular division (mitosis) events in large time-lapse phase-contrast image sequences. To address the challenges induced by non-structured (random) motion, cellular agglomeration, and cellular mitosis, the process of automatic (unsupervised) cell tracking is carried out in a sequential manner, where the inter-frame cell association is achieved by assessing the variation in the local cellular structures in consecutive frames of the image sequence. In our study a strong emphasis has been placed on the robust use of the topological information in the cellular tracking process and in the development of targeted pattern recognition techniques that were designed to redress the problems caused by segmentation errors, and to precisely identify mitosis using a backward (reversed) tracking strategy. The proposed algorithm has been evaluated on dense phase contrast cellular data and the experimental results indicate that the proposed algorithm is able to accurately track epithelial and endothelial cells in time-lapse image sequences that are characterized by low contrast and high level of noise. Our algorithm achieved 86.10% overall tracking accuracy and 90.12% mitosis detection accuracy.

Index Terms— Cell tracking, Delaunay triangulation, cellular interaction, mitosis, time-lapse microscopy.

I. INTRODUCTION

CELL migration is one of the key cellular processes that is associated with a wide range of biological phenomena including embryogenesis, inflammation, wound healing, tumour development [1], [2], and its accurate estimation plays an important role in cell and molecular biology research [3]. Typically, cell migration is evaluated in time-lapse image data and the current practice involves a labour intensive (manual) procedure that is applied to analyze/track the cells in all frames of the image sequence. With the advent of modern microscopy imaging modalities the amount of information required to be analyzed by clinical experts has substantially increased and in many situations the standard manual

procedure has become impractical [2]. The limitations of the manual procedures when applied to the estimation of cell migration opened a new research area that addresses the development of computer vision-based automatic cellular tracking algorithms.

Automatic cellular tracking is challenging due to several factors such as low image contrast, changes in the morphology of the cells over time, random migration, cell division [19], [27], [28], cell interaction [7] and low signal to noise ratio. These challenges vary to a great extent depending on the characteristics of the imaging systems or on the nature of the cell lines being analyzed, and as a result numerous semi-automatic [4]-[6] and fully automatic [1], [8], [11] cell tracking algorithms were proposed in the literature. When the published algorithms are evaluated from a computer vision standpoint, two main categories can be identified. Thus, the first category of cell tracking algorithms includes segmentation-driven approaches [1], [4], [7]-[9], [20], [30], [31], while the second category comprises model-based approaches that typically are either based on contour propagation [5], [11]-[17] or on the combination between intensity/shape models and motion prediction (using Kalman and particle filtering) [10], [17], [18]. Among these two categories, the segmentation-driven cell tracking strategies proved more successful when applied to phase-contrast cellular data [26], [29] due to their improved resilience to variations in imaging conditions, high cell density, cellular agglomeration, cellular division and sudden changes in cell morphology. During the development of cell tracking techniques for phase-contrast cellular-data, the main issues are associated with the avoidance of cell segmentation errors and the implementation of robust association rules that are able to enforce the continuity of the tracking process in the spatio-temporal domain in the presence of cellular division.

In this context, the major objective of this paper is to describe the implementation of a fully automatic cell tracking framework that has been specifically designed to address the identification of the cell lineages and detect mitosis in dense time-lapse phase-contrast cellular data. In the proposed framework, the cells are segmented in each frame using a multi-phase adaptive algorithm and the cell association process is carried out by evaluating the topology of the local cell structures in consecutive frames of the sequence. In our implementation the connectivity rules between neighbouring cells are encoded using Delaunay triangulation [21]. Since the

This work was supported by the National Bio-photonics and Imaging Platform (NBIP) Ireland funded under the Higher Education Authority PRTL Cycle 4, co-funded by the Irish Government and the European Union - /Investing in your future/.

K. Thirusittampalam is with the Center for Image Processing and Analysis, Dublin City University, Ireland. (phone: 353-1-700-7636; fax: 353-1-700-5508; e-mail: thirusittampalm.ketheesan2@mail.dcu.ie).

M. J. Hossain, O. Ghita, and P. F. Whelan are with the Center for Image Processing and Analysis, Dublin City University, Ireland. (e-mail: julius.hossain@dcu.ie, ghita@eeng.dcu.ie, and paul.whelan@dcu.ie).

phase-contrast cellular data that is evaluated in this study is characterized by large contrast variation and a relative high level of noise, the identification of the cells throughout the sequence proved quite difficult. To compensate for the segmentation errors we have developed a novel approach based on the evaluation of the alterations in the local cellular structures which proved capable of detecting and correcting the errors caused by under-segmentation, with sizeable improvements in relation to tracking accuracy. The last component of the proposed algorithm addresses the mitosis detection using a hybrid implementation that combines the backward tracking analysis with the application of normalized cross correlation for the identification of the child cells that were missed by the forward tracking phase of the algorithm. The experimental tests have been performed using in-vitro time-lapse phase contrast image sequences. While the major contributions that emerge from our work are associated with the proposed computational framework that has been designed to address cellular tracking and mitosis detection, we would like to mention that another important contribution is given by the detailed evaluation of our algorithm when applied to various cell-specific data and in the comparative analysis that investigates the performances obtained by our framework and other related cell tracking algorithms.

II. OVERVIEW OF THE PROPOSED TRACKING FRAMEWORK

To facilitate the development of a flexible and efficient cellular tracking solution, the proposed framework is constructed in a multi-step fashion. It involves a hybrid segmentation-driven and pattern recognition-based implementation and the main computational modules of the proposed algorithm are shown in Fig. 1. In this section we will explain the role of each module shown in Fig. 1 and we will briefly introduce the main challenges that have been addressed in the implementation of the proposed cell tracking and mitosis detection algorithm.

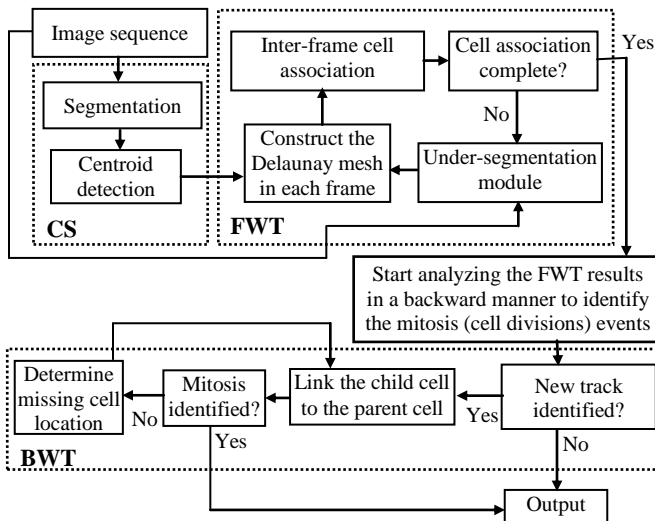


Fig. 1. Overview of the developed cell tracking framework.

As Fig. 1 illustrates, the first component of our algorithm is

the Cell Segmentation (CS) module, which consists of a greyscale morphology-based procedure that is applied to extract the centroids of the cells in each frame. This information is passed to the Forward Tracking (FWT) module, which initially constructs a Delaunay mesh in each frame that encodes the connectivity rules with respect to the positions of the cells in the image. The next step of the FWT module applies the inter-frame cell association process (see Fig. 1). In our implementation, the cell association task is carried out in a sequential manner for pairs of consecutive frames in the sequence, by evaluating the local cell structure in the corresponding Delaunay meshes. Due to inter-frame intensity variations, there are situations when cells in the next frame are not detected by the CS module, and this generates incomplete tracking results where cells in the current frame are left un-associated. To redress the problems generated by cell segmentation errors, the algorithm passes the coordinates of the un-associated cells in the current frame to the *under-segmentation* module. The developed *under-segmentation* module applies an intensity-driven normalized cross correlation approach to identify candidate locations for the undetected cells in the next frame. The candidate locations that minimize the distortions with respect to the local cellular structure of the corresponding cells in the current frame are used to complete the cell association process (for full details refer to Section III.C). The application of the FWT module generates tracking results where the number of tracks progressively increases with the observation time due to the occurrence of cell division (mitosis) events.

Thus, the last component of the proposed cell tracking algorithm, the Backward Tracking (BWT) module, deals with the detection of the mitosis events by analysing the results returned by the FWT in a reversed manner. To robustly address the situations where child cells are missed in the frames that follow mitosis (cellular division), the BWT process is formulated as a combination of pattern matching and inter-frame Delaunay mesh consistency. As indicated in the explanations provided for the FWT module, it is useful to recall that the cell association process involves one to one cell correspondence. Hence, in the presence of cellular division, the parent cell will be associated with one of the child cells, while the remaining child cell will generate a new cell track. The BWT module has been designed to deal with this tracking scenario. Specifically, the BWT module applies a backward sequential search process to identify the parent-child cell links for all tracks resulting from the FWT stage, which provides information not only in regard to cellular migration but also full details about cellular division. In the next section we will discuss in detail all computational modules that are depicted in Fig. 1.

III. THE DEVELOPED CELLULAR TRACKING AND MITOSIS DETECTION ALGORITHM

A. Cell segmentation

The goal of this module is to segment the cells in each frame of the image sequence and to compute their centroid

points that are required to construct the Delaunay mesh. In phase contrast data, the image areas covered by cells have generally a darker interior (nuclei) which is surrounded by a peripheral bright halo [5]. Following this intensity profile model, the cells can be theoretically extracted using threshold-based segmentation techniques. However, our experiments clearly indicated that the application of simplistic thresholding schemes does not provide a robust segmentation option, as the contrast between the cells and background is not constant within the same image and in addition the distribution of the intensity values within the cells areas shows a large degree of variation. Moreover, substantial intensity offsets can be present when the cell data is analyzed in different frames of the sequence, and this issue inserts an additional challenge that has to be addressed by the cell segmentation algorithm. To provide an insight into this problem, Fig. 2(a) shows a section cropped from a phase contrast image containing Madin-Darby Canine Kidney (MDCK) epithelial cells. In Fig. 2(a) it can be observed that the contrast between the cells and background is shallow and this fact is further emphasized in Fig. 2(b) where the corresponding histogram is displayed. To factor in the complications outlined in Fig. 2(b), we have developed a cell segmentation scheme that is able to accommodate the shifts in the intensity domain and to maximally exploit the contrast difference between the cells and the background information. In this regard, the cell regions are highlighted by generating intensity peaks around the cells' nuclei by applying a method that is primarily based on the extended maxima transform [22].

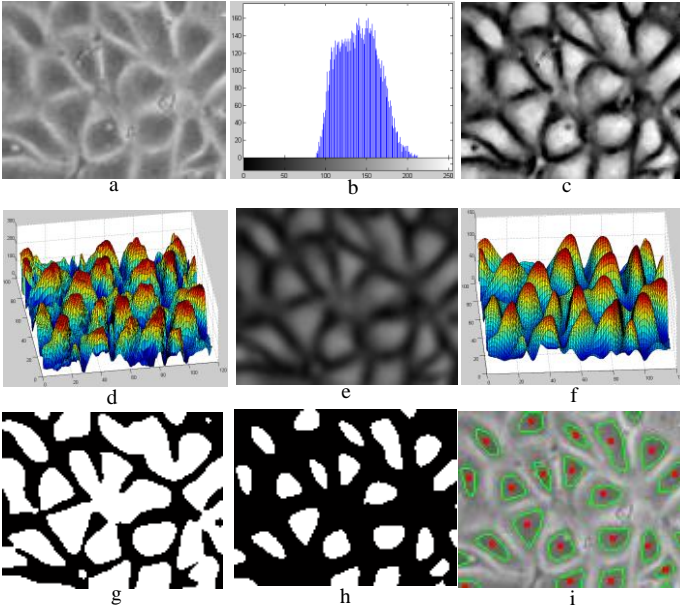


Fig. 2. The process of cell segmentation. (a) An image section taken from a phase contrast image. (b) Histogram of the image section shown in (a). (c) I_{TH} - top-hat transformed image. (d) 3D plot of the intensity map for I_{TH} . (e) Gaussian smoothed data - I_{σ} . (f) 3D plot of the intensity map for I_{σ} . (g) Segmentation results using a standard adaptive threshold approach [23]. (h) Segmentation result obtained by the proposed method. (i) The borders and the centroids of the segmented cells (for clarity purposes they are overlaid on the input image).

The proposed cell segmentation scheme consists of several steps. Initially, the *top-hat* transform is applied to enhance the local contrast, reduce the background noise and the uneven illumination: $I_{TH} = \text{tophat}(\bar{I}, S(r)) = \bar{I} - (\bar{I} \circ S(r))$, where \bar{I} is the inverted input image, I_{TH} is the top-hat transformed image and $S(r)$ is a circular structuring element. The radius r is experimentally determined using the constraint that the structuring element should be larger than the cell nuclei. This condition ensures that all cellular structures that are present in the image are preserved. The output of the top-hat transform when applied to the image data shown in Fig. 2(a) is depicted in Fig. 2(c). As illustrated in Fig. 2(d) the application of the top-hat transform increases the contrast between the cell nuclei and the background, but it can be observed that some noisy peaks are still present in the top-hat transformed image (I_{TH}). This image also details situations where several local peaks are located inside the area covered by a single cell. To remove these problems, the data resulting from the top-hat transform is smoothed using a Gaussian filter and the result is shown in Fig. 2(e). In our implementation, to efficiently suppress the noisy peaks inside the cell, we set the scale σ of the Gaussian filter to r . To illustrate the inappropriateness of the standard thresholding approaches when applied to the segmentation of phase contrast cellular data, the adaptive scheme detailed in [23] has been applied to the Gaussian smoothed image, I_{σ} , and the result is shown in Fig. 2(g). Fig. 2(g) indicates that the application of the adaptive thresholding method generates a binary data where only one blob was identified. This result clearly highlights the limitations of the threshold-based methods when applied to dense cellular data where the transitions between the cells' nuclei and the background are very shallow. In our approach, to detect the cells' nuclei we applied the extended maxima transform, which is the regional maxima of the h -maxima transform - the value of h is experimentally determined (in our studies the segmentation algorithm has shown good stability when the value of the parameter h has been set in the interval [10, 19] - for more details in regard to the selection of the parameter h refer to Table 1, Section IV). Fig. 2(h) shows the result obtained after the application of the extended maxima transform which provides an accurate segmentation of the cells' nuclei. For clarity purposes, in Fig. 2(i) the cells borders (marked in green) and their centroids (marked in red) are overlaid on the input image.

Additional results that illustrate the performance of the developed morphological-based cell segmentation algorithm in the presence of cellular agglomeration are presented in Fig. 3. The next subsection presents a pseudo-code sequence where the main steps of the proposed cell tracking and mitosis algorithm are outlined.

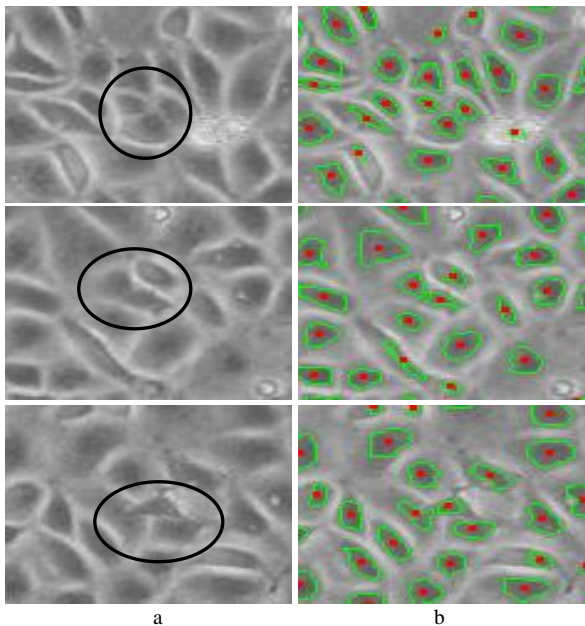


Fig. 3. Cell segmentation results in the presence of cell agglomeration. (a) Image sections cropped from three MDCK datasets. (b) Cell segmentation results. For visualisation purposes, cellular agglomeration cases are marked with black ellipses in images shown in column (a) and the borders and centroids of the segmented cells are overlaid on the results shown in column (b) with green contours and red dots, respectively.

Pseudo-code detailing the main steps of the proposed cellular tracking and mitosis detection algorithm

A. Apply cell segmentation to all frames of the sequence.

Forward Tracking steps

B. Forward tracking (FWT) cell association (frames T and $T+1$)

- B1. Construct Delaunay meshes in frames T and $T+1$
- B2. Evaluate the local structure (triangle) matching using equation (4)
- B3. Associate cells that have their local structures completely matched
- B4. Generate the reference nodes list R
- B5. Associate cells for which $MC(.) < 1$ (cells with local structures partially matched) using equation (8) and add them to the list R
- B6. For each unassociated cell in image T (due to under-segmentation)
 - B6.1. Find the corresponding location for each unassociated cell in frame T by applying normalized cross correlation and the use of local structure in frame $T+1$ (activation of under-segmentation module).

Repeat steps B1 to B6 until the last image in the sequence is processed and generate the forward tracking (FWT) results.

Backward Tracking steps

C. Mitosis detection – perform backward tracking for all tracks TK_i identified by FWT

- C1. Identify the first frame (frame T) associated with the track TK_i (frame in which the cell that generated the track TK_i was detected first)
 - If: frame $T-1$ is the first frame of the sequence: End the analysis for track TK_i (the track is complete from first to last frame of the sequence)
 - Else: Go to step C2
- C2. Apply backward cell association from image T to image $T-1$
- C3. If: no suitable parent cell is identified in frame $T-1$: activate the under-segmentation module to determine the location of the undetected cell in frame $T-1$
 - C3.1 Repeat step C3 in frames $T-2$, $T-3$, etc. until the parent cell is identified
 - Else: Parent cell identified in frame $T-1$

Repeat steps C1 to C3 until all TK_i tracks identified by FWT are processed.

Full details for FWT and BWT modules are provided in Sections III.B and III.C, respectively.

B. Forward tracking module (FWT)

The cell association in dense phase-contrast cellular data represents a challenging task since cells have similar intensity and shape characteristics and the cell migration is defined by random motility patterns. Thus, a cell tracking framework that implements the association process using feature-matching or relies on the information supplied by model-based motion estimators is likely to return inaccurate results. To circumvent the issues relating to feature ambiguity or inconsistent motion estimation, the proposed tracking framework evaluates the structural (topological) relationships among neighbouring cells in the inter-frame cell association process. To provide a compact representation that encompasses the spatial arrangement between neighbouring cells, we employed Delaunay triangulation to generate a unique planar graph that is independent on the topology of the nodes [21], [24]. In our algorithm we have used Delaunay triangulation since this graph-based representation maximizes the minimum angles of the triangles that generate the mesh. In this representation the triangles tend towards equiangularity and the insertion or removal of a node affects the mesh representation only at the local level. This property is particularly appropriate to encode the neighbouring relationship between cells in the image, as the insertion and the removal of nodes can be caused by cellular division or under-segmentation. In the proposed algorithm each node of the mesh represents a cell position that is given by its centroid, and the edges constructed for each node during triangulation define the spatial relationship between the analyzed cell and the cells situated in its close neighbourhood. Using this representation, the node (cell) association process can be efficiently formulated as a graph matching problem, where the local structures associated with the nodes in the Delaunay mesh are analyzed in consecutive frames of the image sequence. Since the local inter-cell relationships are accurately modelled in this formulation, the similarity between the local Delaunay structures in two consecutive frames can be efficiently estimated based on the assumption that cells can be accurately detected in each frame. However, as indicated in Section III.A, when dealing with dense phase-contrast data there are situations when cells are missed by the segmentation process and this generates substantial changes in the local structure that is encoded by the Delaunay mesh. While the cellular association process proposed in our paper is based on the evaluation of the local structure, missing cells in one frame will have a negative effect on the accuracy of the tracking process. This is obvious as the cellular association entails a sequential process, and the incidence of under-segmentation creates discontinuities in the cell lineages that are determined for each individual cell. To overcome this problem, in our implementation we have developed a procedure (referred to as *under-segmentation module*) which determines the location of the missed cell using an intensity-based pattern matching strategy.

Cell association

The correspondence between the cells in frames T and $T+1$ of the image sequence is determined based on the local structure associated with the cells in their neighbourhood graphs D^T and D^{T+1} , respectively, that are obtained using Delaunay triangulation, as explained in Section III.B. If we consider a node (cell centroid) u from mesh D^T , then the local structure associated with u is defined as follows:

$$S_u^T = \{\Delta_{upq} \mid p, q \in D^T, p \perp q, p \perp u, q \perp u\} \quad (1)$$

where $p \perp q$ is a topology operator that denotes that the node with the index p is adjacent to the node with the index q , Δ_{upq} defines the triangular structure that is generated by the u, p, q nodes and $\{\cdot\}$ is the mathematical set operator. To aid the understanding of the mathematical formalism detailed in (1), Fig. 4 depicts a section of the Delaunay mesh that is constructed using the centroids of the cells detected in image T . In this diagram, the local structure associated with the node u is $S_u^T = \{\Delta_{uab}, \Delta_{ubc}, \Delta_{ucd}, \Delta_{ude}, \Delta_{uef}, \Delta_{ufa}\}$.

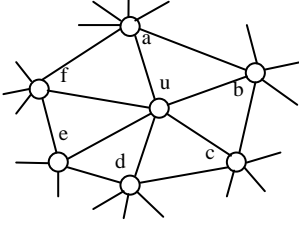


Fig. 4. A section of the Delaunay mesh that illustrates the construction of the local structure S_u^T for the node with the index u .

Now, let S_v^{T+1} be the local structure associated with the node $v \in D^{T+1}$ in the Delaunay mesh that is constructed using the detected centroids in frame $T+1$. At this point we need to define a metric that is able to sample the similarity in the local structures that are associated with the two nodes $u \in D^T$ and $v \in D^{T+1}$. To achieve this goal, we propose to evaluate the structural similarity between S_u^T and S_v^{T+1} in terms of the similarity among the triangles and the edges that are associated with the nodes u and v in frames T and $T+1$, respectively. Thus, the similarity between two triangles is defined according to the Hausdorff distance, which records the largest of all the displacements between one node in one triangle to the closest node in the other triangle. If Δ_1 and Δ_2 represent two triangles, then the Hausdorff distance between these triangles is defined as follows:

$$H(\Delta_1, \Delta_2) = \max\{\varphi(\Delta_1, \Delta_2), \varphi(\Delta_2, \Delta_1)\} \quad (2)$$

where $\varphi(\Delta_1, \Delta_2) = \max_{p \in \Delta_1} \left\{ \min_{q \in \Delta_2} \{d(p, q)\} \right\}$, and $d(p, q)$ is the Euclidean distance between the two nodes with indexes p and q . With respect to (2), the triangles Δ_1 and Δ_2 are assumed to be similar only if their Hausdorff distance is smaller than a predefined threshold α as illustrated in (3) (a perfect match between Δ_1 and Δ_2 is achieved when the Hausdorff distance $H(\Delta_1, \Delta_2) = 0$, i.e. when the corresponding nodes of Δ_1 and Δ_2

have the same coordinates in frames T and $T+1$. An increase in the value of $H(\Delta_1, \Delta_2)$ indicates more dissimilarity between Δ_1 and Δ_2). Since changes in the local structures that are associated with corresponding nodes in frames T and $T+1$ are caused by cell migration, in our implementation the similarity between two triangles $MT(\Delta_1, \Delta_2)$ is evaluated in conjunction with a parameter α , which is set as the maximum instantaneous cell movement in two consecutive frames.

$$MT(\Delta_1, \Delta_2) = \begin{cases} 1, & H(\Delta_1, \Delta_2) \leq \alpha \\ 0, & \text{otherwise} \end{cases} \quad (3)$$

As indicated in (1), the local structure associated with each node consists of a set of triangles that are generated by the node of interest and the adjacent nodes in the Delaunay mesh. Thus, to completely evaluate the similarity between the nodes $u \in D^T$ and $v \in D^{T+1}$, we introduce a matching confidence function $MC(\cdot)$ that evaluates the similarity between two local structures S_u^T and S_v^{T+1} , where the similarity between two triangles is evaluated using (3).

$$MC(u, v) = \frac{\sum_{\Delta_i \in S_u^T, \Delta_j \in S_v^{T+1}} MT(\Delta_i, \Delta_j)}{\max(\|S_u^T\|, \|S_v^{T+1}\|)} \quad (4)$$

where $\|S_u^T\|$ represents the number of triangles contained in the set S_u^T . In (4) the numerator evaluates the similarity between the two sets of triangles contained in the local structures S_u^T and S_v^{T+1} , while the denominator is applied to normalize the matching confidence, $MC(\cdot)$ values, in the range $[0, 1]$. With respect to the value of the matching confidence returned for each pair of nodes (cells) in frames T and $T+1$, the cells are associated in multiple stages. In the first stage the nodes (cells) in frames T and $T+1$ that have complete structure similarity (i.e. $MT(\cdot) = 1$ for all triangles in the local structures S_u^T and S_v^{T+1}) are associated. This situation is illustrated in Figs. 5(a) and 5(b) where two nodes $u \in D^T$ and $v \in D^{T+1}$ have their structures completely matched. All nodes $p \in D^T$ and $q \in D^{T+1}$ that have their local structures completely matched (i.e. are associated in the first stage) are included in a reference list R as follows:

$$R = \{(p, q) \mid p \in D^T, q \in D^{T+1}\} \quad (5)$$

where p and q form a matched pair.

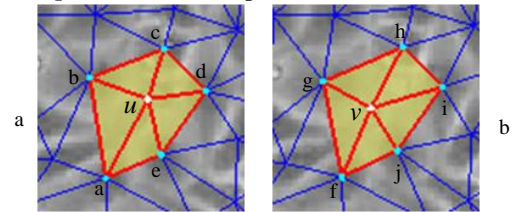


Fig. 5. Example showing two nodes u and v in frames T (a) and $T+1$ (b) that have their local structures $S_u^T = \{\Delta_{uba}, \Delta_{uac}, \Delta_{ued}, \Delta_{ude}, \Delta_{uceb}\}$ and $S_v^{T+1} = \{\Delta_{vgf}, \Delta_{vji}, \Delta_{vih}, \Delta_{vhg}\}$ completely matched using (4) and included in the list R .

The nodes included in the list R are the nodes (cells) that are associated with the highest confidence and they will be used in the following stages of the cell association process - when we attempt to associate the nodes for which the local structure was only partially matched. In the second step, for nodes with $MC(\cdot) < 1$ that have in their local structure at least a pair of matched nodes included in the list R , we calculate the partial matching confidence $PMC(\cdot)$, using (8), that evaluates both the similarity for triangles and mesh edges with respect to the reference nodes containing in the list R . In this node association stage we also evaluate the distance between the nodes to place a higher degree of confidence when matching the nodes with $MC(\cdot) < 1$. The last term in (8) penalises the large displacements of the node v in frame $T+1$ with respect to the position of the node u in frame T . The reference edge structure associated with $u \in D^T$ is defined as:

$$E_u^T = \{\overline{up}\} | p \in R, p \perp u \quad (6)$$

Similarly, the reference edge structure associated with $v \in D^{T+1}$ is defined as:

$$E_v^{T+1} = \{\overline{vq}\} | q \in R, q \perp v \quad (7)$$

The $PMC(\cdot)$ is calculated as follows:

$$PMC(u, v) = MC(u, v) + \frac{ME(E_u^T, E_v^{T+1})}{\max(\|E_u^T\|, \|E_v^{T+1}\|)} + \left(1 - \frac{d(u, v)}{\alpha}\right) \quad (8)$$

where $ME(E_u^T, E_v^{T+1})$ represents the number of matched edges between E_u^T and E_v^{T+1} , and $\|E_u^T\|$ denotes the number of edges in the set $\{E_u^T\}$. The nodes that maximize the value of $PMC(\cdot)$ are associated and they are included in the list R .

Fig. 6 illustrates two scenarios where corresponding nodes in two consecutive frames have their local structures only partially matched using (4). In the first scenario (Figs. 6(a) and 6(b)) the local structure is distorted mostly due to the under-segmentation of the cell f (marked with a brown circle in Fig. 6(a)) in frame $T+1$. In the second scenario (Figs. 6(c) and 6(d)) the local mesh distortion is generated by the large random motion of the cells. In this figure the triangles that are matched using (3) are displayed in yellow (for visualization purposes are also marked with black dots) and the matched edges are shown in red. The nodes that are still left un-associated in the current frame after the application of the second stage of the tracking process did not find a corresponding cell in the next frame ($T+1$) due to either under-segmentation or to situations where the corresponding cells in the next frame have exited the region of interest that is imaged by the microscope. While the nodes in frame T for which the corresponding nodes in frame $T+1$ left the region of interest were correctly left un-associated, in the last stage of the cell association process we will focus on the nodes (in frame T) that were not associated due to under-segmentation that occurs when nodes in frame

$T+1$ were not detected by the segmentation process. This last stage of the FWT will be explained in the next section.

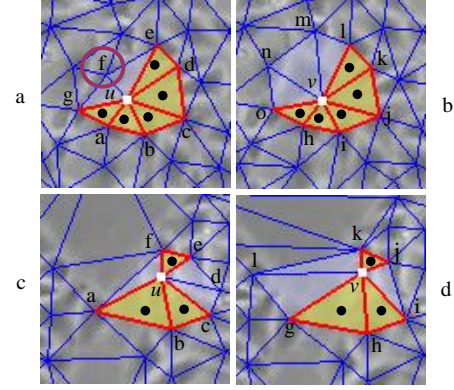


Fig. 6. The association of the nodes for which the local structure was partially matched. (a) and (b) Partial matching for nodes u and v in frames T and $T+1$ that is caused by under-segmentation (no corresponding cell has been segmented in frame $T+1$ for the cell f (marked with a brown circle) in frame T). (c) and (d) Example that illustrates the partial matching of the local structures s_u^T and s_v^{T+1} , in frames T and $T+1$ due to large random motion. The triangles that are matched using (3) are displayed in yellow and marked with black dots. This diagram is best viewed in color.

Handling under-segmentation

During the segmentation process there are situations where cells are not detected by the h -maxima-based algorithm due to the faint intensity contrast between the cell area and the background. The occurrence of under-segmentation in frame $T+1$ has negative consequences, as it largely affects the local structure in the Delaunay mesh. As a consequence of these disturbances in the local cell topology, the corresponding cells in frame T are left un-associated after the application of the two-stage FWT process (for details please refer to the explanations provided in the previous section). Fig. 7 illustrates a practical example that is caused by under-segmentation, where the segmentation algorithm has missed the corresponding cell in frame $T+1$ for the cell labelled with u in frame T (see Fig. 7(a) and 7(b)). To better illustrate the effects of under-segmentation on the tracking process, Figs. 7(c) and 7(d) depict the tracking results for frames T and $T+1$, respectively, where the cell with the index 103 in Fig. 7(c) (which is the cell u in Fig 7(a)) was left un-associated and the tracking of this cell is terminated as indicated in Fig. 7(d) (there is no cell with the track index 103 in frame $T+1$). Since the FWT process is applied in a sequential manner, if this under-segmented cell is detected after a few frames, it will be treated as a new cell and the FWT algorithm will erroneously assign a new track index. Thus, the identification of under-segmentation plays a critical role in obtaining tracking results with no gaps in the resulting cell lineages. If cells are left un-associated in frame T , this triggers the activation of the procedure that is applied to redress the problems caused by under-segmentation. The proposed method attempts to identify a location in frame $T+1$ for each cell in frame T that has not been associated in the first two stages of FWT.

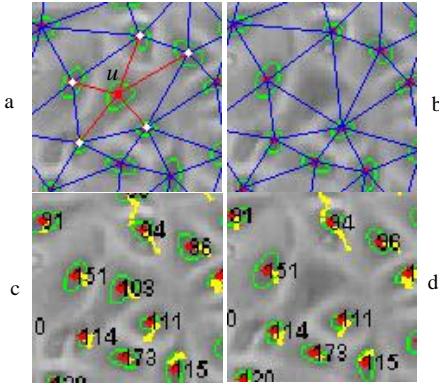


Fig. 7. The effects of under-segmentation on tracking results. (a)-(b) Sections cropped from frames T and $T+1$ with the Delaunay mesh overlaid on the intensity data. (c)-(d) Cell association results for frames T and $T+1$. Note that the under-segmentation in frame $T+1$ corresponding to the cell u in frame T causes the incorrect termination of the track with the index 103.

The developed algorithm applies *normalized cross correlation* [25] to locate in frame $T+1$ a pattern that approximates the intensity profile of the rectangular mask that encompasses the area of the un-associated cell in frame T . To avoid the potential identification of cell locations that are too far from the un-associated cell in frame T , the search space in frame $T+1$ is restricted within $W = (2\alpha+1) \times (2\alpha+1)$ area whose centre is the location of the centroid of the un-associated cell (the parameter α has been introduced in (3) and it is set as the maximum instantaneous cell movement in two consecutive frames). Since there are several patches within the W search space that closely approximate the intensity profile of the mask image, the application of normalized cross correlation generates multiple peak points. Among all peak locations in frame $T+1$, the one that maximizes the similarity with the local structure present in frame T is selected as the best candidate location in frame $T+1$ for the un-associated cell in frame T . In our implementation the local structure dissimilarity is measured using (9), where the local structure in frame $T+1$ is constructed by connecting the associated cells and the selected peak location.

$$DL(u, v_i) = \frac{\sum_{(a,b) \in R} |l(\overline{ua}) - l(\overline{v_i b})|}{\max_{(a,b) \in R} (l(\overline{ua}), l(\overline{v_i b}))} + \frac{\sum_{(a,b) \in R} |\theta(\overline{ua}) - \theta(\overline{v_i b})|}{\max_{(a,b) \in R} (\theta(\overline{ua}), \theta(\overline{v_i b}))} \quad (9)$$

where $\overline{ua} \in D^T$, $\overline{v_i b} \in D^{T+1}$, $l(e)$ defines the length of the edge e and $\theta(e)$ represents the angle of the edge e with respect to the horizontal axis. In (9), $DL(u, v_i) \in [0, 2]$ measures the local mesh distortion between the local structure of the un-associated cell u in frame T and that associated with the candidate peak v_i in frame $T+1$. As previously indicated, the peak that minimizes the output of (9) is selected as the missing cell location in frame $T+1$.

$$v = \arg \min_{v_i | i \in [1, m]} DL(u, v_i) \quad (10)$$

where m defines the number of candidate peaks that are selected using the normalized cross correlation. The step-by-

step operations that are applied to redress the problems caused by under-segmentation in Fig. 7 are illustrated in Fig. 8. Fig. 8(a) shows the node u in image T , which was left un-associated due to under-segmentation. The candidate points v_1 , v_2 and v_3 that are identified by the normalized cross correlation procedure in frame $T+1$ are displayed in Fig. 8(b). Figs. 8(c)-(e) depict the mesh edges (marked with red lines) that are obtained for each of these candidate locations when the Delaunay triangulation is regenerated in frame $T+1$. All new structures generated by the candidate points are compared with the local structure of the un-associated node in frame T (see Fig. 8(a)) using (9), and the corresponding distortions $DL(u, v_i)$ that are obtained for the candidates points (v_1, v_2, v_3) shown in Fig. 8(b) are 0.5, 1.8 and 1.3, respectively. By applying (10), the node v_1 (Fig. 8(c)) that returns the minimum value is selected as the corresponding location in frame $T+1$ for the un-associated cell u .

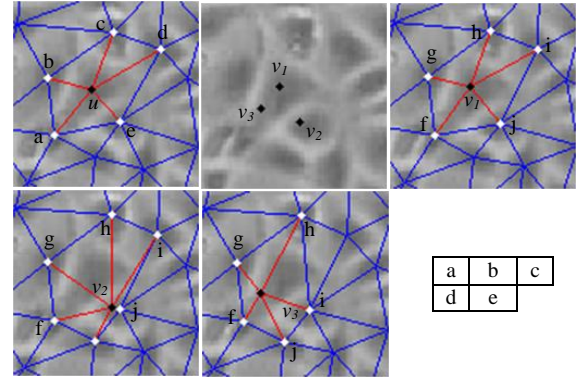


Fig. 8. Identification of the missing cell location. (a) The local structure of the un-associated node u in frame T . (b) Candidate points in frame $T+1$. (c)-(g) Local structures associated with each of the detected candidate points that are obtained after the application of the Delaunay triangulation in frame $T+1$. The candidate v_1 returns the minimum local distortion $DL(\cdot)$ and is selected as the corresponding location in frame $T+1$ for the cell u in frame T .

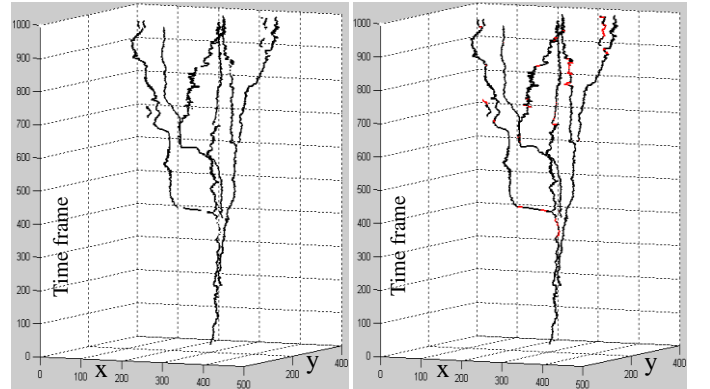


Fig. 9. Tracking results displayed in a 2D+t graph. (a) Cell trajectories in the absence of the under-segmentation module. (b) Cell trajectories in the presence of the under-segmentation module. This diagram is best viewed in color.

Fig. 9 shows the cell lineages (trajectories) calculated for a single MNP cell and its descendents that are generated by mitosis over 1000 frames. For clarity purposes the data is displayed as a 2D+t graph. To illustrate the undesirable effect of the segmentation errors on the tracking results, we have deactivated the module designed to redress the problems caused

by under-segmentation and the tracking results are depicted in Fig. 9(a). In Fig. 9(a) it can be clearly observed the significant number of breaks in the tracking results that are caused by the segmentation errors. To graphically illustrate the increase in performance that is induced by the method designed to compensate for the errors introduced by the segmentation process, the cell trajectories calculated when the under-segmentation module is activated are shown in Fig. 9(b). For illustrative purposes, the tracks that are identified by the proposed method are marked in red and this diagram illustrates the significant improvements in terms of tracking continuity when compared to the results shown in Fig. 9(a). In Fig. 9(b) the new tracks that are generated by mitosis (cell division) can also be observed and in the next section we will detail an algorithm that has been designed to detect mitotic cells using a backward tracking strategy.

C. Backward tracking module (BWT)

Mitosis is the process by which a parent cell divides into two similar cells called child or daughter cells. Since the frequency of the mitosis events plays an important role in achieving accurate and complete tracking results, in our work we developed an automatic approach to detect the cell division using a backward tracking strategy, which links the child tracks to the corresponding parent cell. Due to intensity variation and poor contrast in phase contrast image sequences, child cells are not assured to be detected in all frames. Since the mitosis events are not *a priori* known during the forward tracking process, the parent cell will be linked to one of the child cells after cell division (i.e. one of the child cells will have the same track index as the parent cell), while the other child cell which remains un-associated will generate a track with a new index. Thus, the detection of mitosis during forward tracking will be quite problematic, and this is especially true when dealing with cellular data which does not exhibit conspicuous intensity transitions in the frame that precedes cellular division. To robustly detect the mitotic events, especially when dealing with situations when the child cell was missed by the segmentation process, we applied a multi-stage backward tracking process. During backward tracking, the proposed algorithm determines the location of the missed child cells (if necessary) and evaluates in a reverse manner all tracks determined during FWT with the goal of finding the new tracks that are generated by the cellular division events. After the application of BWT for each cell in the dataset, a complete tree structure over the entire image sequence will be generated, where each branch is associated with a mitosis event. Fig. 10 illustrates the cell division process where a parent cell divides in frame T . As indicated earlier, one of the child cells (child cell-1) is tracked with the parent ID (TK_1) during FWT, while the child cell-2 is detected by the segmentation module in frame $T+2$ and will be tracked in the subsequent frames with a new track index (TK_2). As it can be observed in this diagram, the segmentation algorithm missed the child cell-2 in frame $T+1$ and this fact did not triggered the activation of the under-segmentation procedure detailed in Section III.B as the parent cell has found a match in

frame $T+1$ (child cell-1). Thus, this under-segmentation problem needs to be addressed during backward tracking (BWT). In this regard, the backward tracking module approaches the identification of the missing cell location in frame $T+1$ starting from frame $T+2$ in a reversed manner. To illustrate this process, in Fig. 10 the trajectories analyzed by the backward tracking are marked with a dashed line. This process continues with the identification of the missing cell in frame T . Once the missed cell has been identified (this will be explained later) in frame T , it can be clearly observed that for this cell the corresponding cell in frame $T-1$ is the parent cell that generated the mitosis event.

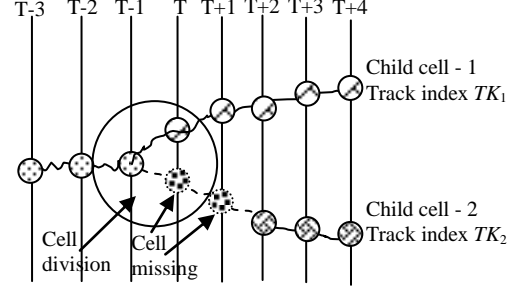


Fig. 10. Diagram detailing the cell division process.

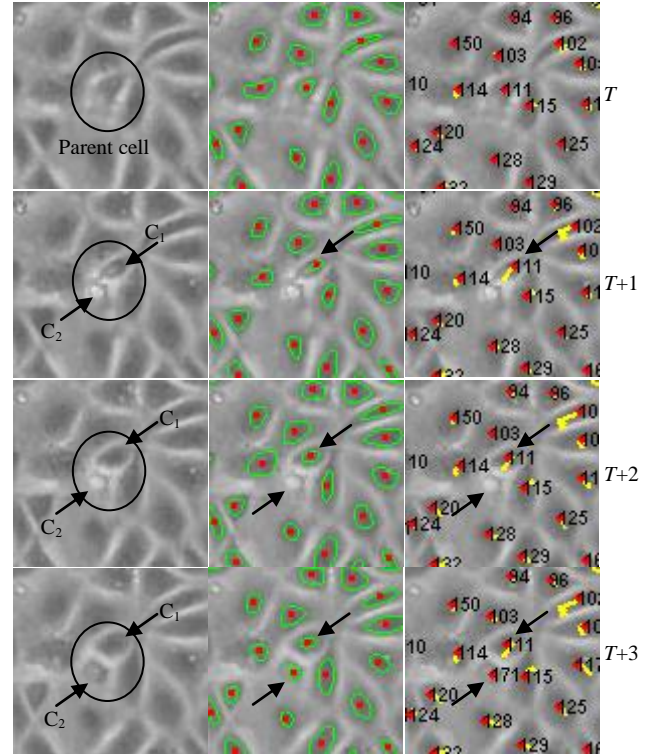


Fig. 11. Forward tracking results in the presence of cell division. In this diagram the results of the forward tracking are shown for four consecutive frames. The child cells resulting from the cellular division are indicated by the black arrows.

Fig. 11 illustrates the forward tracking results for an image sequence that sample a cellular division event. In this diagram, cell-111 shown in frame T divides into two child cells in frame $T+1$ where one child cell is tracked with the same index as the

parent cell (111) in the subsequent frames of the sequence. The other child is missed in frames $T+1$, $T+2$ and is detected only in frame $T+3$ by the segmentation algorithm, and it is tracked in the subsequent frames with a new track index (171). The application of the backward tracking determines the missing cell location for the under-segmented child cell in a sequential manner, initially in frame $T+2$, and then in frame $T+1$, and finally the BWT links the track with the index 171 to the parent track with the index 111 in frame T .

In the remainder of this section we will provide a step-by-step description of the BWT process that was graphically outlined in Fig. 10. As indicated earlier, the backward tracking evaluates all tracks returned by FWT in a reverse manner and this process is repeated until we obtain the parent-child links for all new tracks that were generated by cellular divisions. To avoid any erroneous mitosis detection results that are caused by the cells situated near the border of the region of interest (i.e. area imaged by the microscope), these cells are ignored by the backward tracking process as they generate a large number of new short tracks since the border cells frequently exit and re-enter the region of interest.

When analysing the tracks in a backward manner, in situations where the algorithm is not able to locate the parent cell for a new track, we apply a process similar to the one developed to detect the under-segmented cells in the forward direction (see Section III.B), but this time in the reversed direction, i.e. from frame $T+k$ towards frame $T+k-1$. Thus, if the first cell of a new track in frame $T+k$ does not find a parent cell in frame $T+k-1$, then a set of candidate locations ($v_i | i \in [1, m]$) in frame $T+k-1$ are identified by the use of normalized cross correlation within a search region $(2\alpha+1) \times (2\alpha+1)$. Similar to the approach detailed in Section III.B, for each candidate location v_i a local structure is created, the distortion in the local structure is evaluated with (9) and the candidate location which minimize the expression in (9) is selected as the location of the under-segmented cell.

This procedure is sequentially applied to the subsequent frames in a backward direction until the candidate location v overlaps with the location of a cell that has a different track index (this cell is assigned as the parent cell that generated the cell division event). We would like to point out that during the backward tracking process the use of the local structure in the mitosis detection process provides major benefits in terms of accuracy. This is illustrated in Fig. 12 where the structural information for all candidate locations is analyzed in a step-by-step fashion. Fig. 12(a) shows a section cropped from frame T and the aim is to identify the corresponding location for the node u in frame $T-1$. The candidate locations v_i determined using normalized cross correlation in frame $T-1$ are marked with black dots and are shown in Fig. 12(b). Figs. 12(c) to 12(e) illustrate the local structures that are constructed for all candidate points. Fig. 12(f) depicts the location of the best candidate (marked with a blue circle) that has the local structure most similar to the structure associated with the node u in frame T . Figs. 12(g) and 12(h) show the detection of the missing cell location in frames $T-2$ and $T-3$, where we can observe that the analyzed track progressively converges

towards the location of the parent cell with the track index 111.

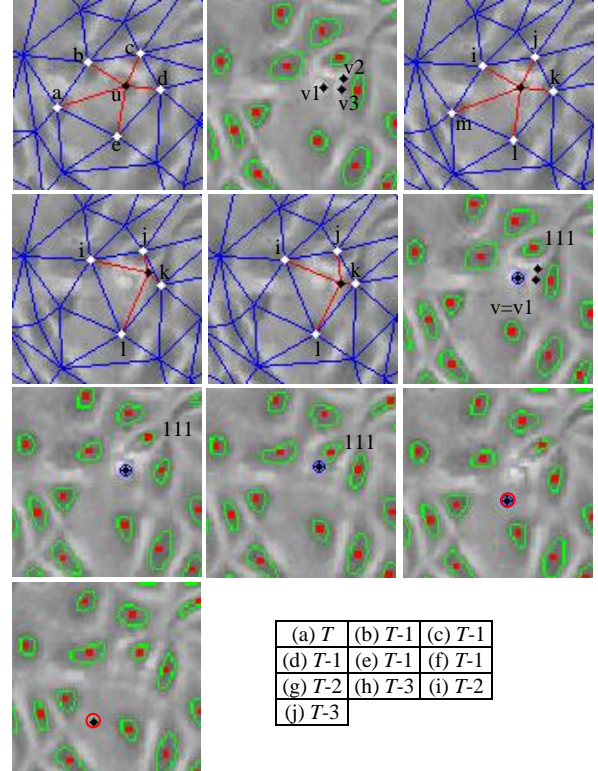


Fig. 12. Detection of the missing cell location during the backward tracking process. (a) The child cell u in frame T for which we seek the identification of the parent cell. (b) Candidate locations in frame $T-1$. (c)-(e) Local structures for all candidate locations. (f)-(h) Detection of the missing cell location using the proposed method in frames $T-1$, $T-2$ and $T-3$, respectively. (i)-(j) Detection of the missing cell location using only normalized cross correlation in frames $T-2$ and $T-3$, respectively. Observe the incorrect results returned by the normalized cross correlation-only approach, while the results returned by the proposed method converge to the correct location of the parent cell.

To illustrate the advantage gained by the enforcement of the local structure in the backward tracking process, Figs. 12(i) and 12(j) show the best locations detected for the under-segmented cell (marked with red circles) in frames $T-2$ and $T-3$, when only the result of the normalized cross correlation is used (the best location for the missed cell is evaluated using only data available in the intensity domain). As illustrated in Figs. 12(i) and 12(j) the use of intensity information alone (using only normalized cross correlation) is prone to substantial errors. In Figs. 12(i) and 12(j) it can be clearly observed that the estimation of the missed cells in frames $T-2$ and $T-3$ is erroneous, as the detected location departs from the location of the parent cell with the index 111 (see Fig. 12(h)).

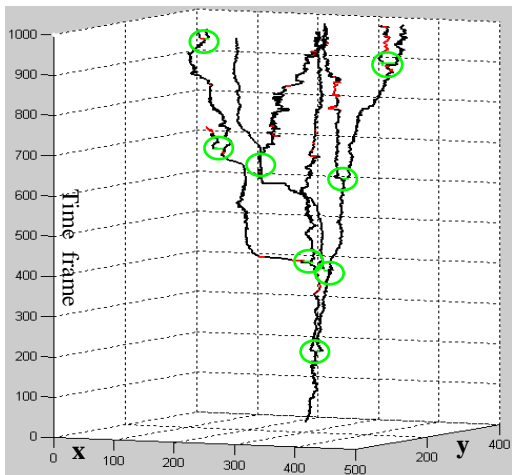


Fig. 13. Trajectories of a tracked MNP cell over the entire image sequence. Mitosis events are marked in green (also indicated by green circles) and the cells trajectories identified by the under-segmentation module are marked in red. This diagram is best viewed in color.

To provide additional results regarding mitosis detection, Fig. 13 shows the trajectories of a MNP cell over the entire (1000 frames) sequence where the links between the parent-child cells are marked in green (for visualization purposes the mitosis events are also marked in Fig. 13 with green circles). The results returned by the FWT and BWT processes allow the calculation of detailed statistics that provide precise indicators about the motility patterns for each cell in the sequence and offer a rich source of information that can be used by the biologists in the estimation of cell proliferation.

IV. EXPERIMENTAL RESULTS

A. Experimental results for MDCK and HUVEC cell lines

The proposed cellular tracking framework is evaluated on several challenging time-lapse phase contrast cell image sequences that are characterized by low image contrast and high level of noise. The results returned by the automatic cell tracking algorithms are compared against the manually annotated data. To further evaluate the performance of the developed method it has also been applied to public available cellular datasets [1], [4] and its performance is compared against those reported by related cell tracking and mitosis detection implementations.

The performance of the proposed method is evaluated with respect to the overall tracking accuracy and the accuracy of the cell division detection. The overall tracking accuracy is given by the number of valid tracks (tracks that are correctly identified with respect to the manually marked data) detected by the proposed method versus the total number of tracks identified in the manually analyzed data. The accuracy of the mitosis detection is defined by the number of cell divisions correctly identified by the proposed algorithm with respect to the total number of cell divisions events present in the manually annotated data. As the proposed tracking and mitosis algorithm has been evaluated on cellular data captured for different cell types with particular intensity domain characteristics, in Table I we present the set of parameters that

were optimised for each category of cellular data.

TABLE I
THE VALUES OF THE PARAMETERS THAT HAVE BEEN OPTIMISED FOR EACH CATEGORY OF CELLULAR DATA USED IN OUR EXPERIMENTS

				Parameters			
Data sets	Cell type	# of sequences	# of frames/sequence	Temporal resolution (min/frame)	r	h	α
	MDCK	3	100	10 to 20	15	19	12
HUVEC	4	323	10	15	15	20	
MNP	3	1000	5	11	10	15	
HeLa	1	100	15	The segmentation results provided in [1] have been used		20	

Table II details the quantitative results when the proposed method has been applied to three MDCK epithelial cell image sequences and four Human Umbilical Vein Endothelial Cells (HUVEC) image sequences. These cellular datasets have a spatial resolution of $1.3\mu\text{m}/\text{pixel}$ and the temporal resolution is 10 min/frame for HUVEC data and in the range 10 to 20 min/frame for MDCK data. In the second column in Table II, the overall tracking accuracy with respect to the manually annotated data is reported, where the values within the brackets denote the number of valid tracks and the total number of tracks, respectively. In the third column of Table II, the accuracy of the cell division detection is reported, where values within brackets indicate the number of cellular divisions that are correctly identified by the proposed algorithm and the total number of cell divisions that were detected in the manually annotated data. For consistency reasons we also report Precision results, where the values within brackets indicate the number of false positives.

TABLE II
QUANTITATIVE RESULTS OBTAINED BY THE PROPOSED CELLULAR TRACKING AND MITOSIS DETECTION METHOD WHEN APPLIED TO MDCK AND HUVEC DATASETS.

Sequence	Tracking accuracy (Recall)	Precision	Mitosis detection accuracy (Recall)	Precision
MDCK-1	89.47% (170/190)	97.14% (5)	85.29% (29/34)	85.29% (5)
MDCK-2	87.50% (105/120)	92.1% (9)	79.17% (19/24)	70.37% (8)
MDCK-3	82.18% (143/174)	92.86% (11)	87.23% (41/47)	78.85% (11)
HUVEC-1	81.48% (44/54)	77.19% (13)	86.67% (13/15)	76.47% (4)
HUVEC-2	78.35% (76/97)	97.44% (2)	100% (12/12)	85.79% (2)
HUVEC-3	82.65% (81/98)	81.82% (18)	95.83% (23/24)	79.31% (6)
HUVEC-4	82.35% (42/51)	85.71% (7)	88.89% (8/9)	72.73% (3)

The overall tracking accuracy achieved by the proposed method when applied to MDCK and HUVEC sequences varies between 78.35% and 89.47%, while the accuracy of the mitosis detection varies between 79.17% and 100%. These quantitative results are encouraging considering that these image sequences are characterized by low image contrast, substantial intensity variations and the density of the cellular structures is high.

B. Additional experimental results using public available cellular data and comparisons with related cell tracking algorithms

To evaluate the performance of the proposed method when compared to other relevant cellular tracking implementations

we applied it to public available datasets for which tracking results have been reported in the literature [1], [9]. To this end, we selected two different types of image sequences of Murine Neural Progenitor (MNP) [4] and HeLa [1] cells. The authors in [9] reported tracking and mitosis detection results for both types of image sequences, and this allows an accurate performance comparison between the results reported in [9] and the results obtained by the proposed method. Comparative results are reported in Table III, and it can be observed that the proposed method outperforms the method detailed in [9] with respect to tracking and mitosis detection when applied to the MNP cell data. When the proposed method was evaluated on HeLa cell data we are in a position to report experimental results for a dataset that contains 100 frames, as only this amount of data has been publicly made available by the authors of [1].

TABLE III
CELLULAR TRACKING AND MITOSIS DETECTION RESULTS WHEN THE PERFORMANCE OF THE PROPOSED METHOD IS COMPARED TO THAT OBTAINED BY THE METHOD DETAILED IN [9].

Sequence	Proposed method			Method presented in [9]		
	#of frames	Tracking	Division	#of frames	Tracking	Division
MNP-1	1000	89.47%	94.12%	1000	87.31%	83.76%
MNP-2	1000	91.30%	91.67%	1000	85.21%	84.62%
MNP-3	1000	88.64%	90.00%	1000	84.43%	82.85%
HeLa	100	93.75%	92.5%	500	85.01%	82.68%

The next experiments analyzes the accuracy obtained by our method and that obtained by the method presented in [1] when both methods are applied to HeLa cell data. The authors in [1] reported experimental results when they applied their cell tracking approach to four sequences, where each sequence contains 200 frames. As noted earlier, we are able to report experimental results for only one sequence that contains 100 frames, as only this amount of data is available in the public domain. To allow a direct evaluation for both methods we used the same performance metrics that were employed by the authors in [1] to evaluate the tracking accuracy.

TABLE IV
CELLULAR TRACKING RESULTS WHEN THE PERFORMANCE OF THE PROPOSED METHOD IS COMPARED TO THAT OBTAINED BY THE METHOD DETAILED IN [1].

Error type	Proposed method	Method presented in [1]			
	HeLa (100 frame)	HeLa-1 (200 frames)	HeLa-2 (200 frames)	HeLa-3 (200 frames)	HeLa-4 (200 frames)
ETR	6.25%	7.22%	14.68%	8.41%	9.16%
EMR	9.00%	6.18%	13.76%	8.41%	8.40%

In [1] the authors evaluated the tracking accuracy using the Error Trace Rate (ETR) and Error Matching Rate (EMR). ETR is defined as the number of track errors divided by the total number of tracks, where EMR is defined as the number of individual matching errors recorded in all detected tracks divided by the total number of tracks [1]. The experimental results are presented in Table IV. The results for ETR and EMR in [1] vary from 7.22% to 14.68% and 6.18% to 13.76%, respectively, while ETR and EMR values calculated for the proposed method are 6.25% and 9%, respectively. The experimental results presented in Tables II to IV indicate that the proposed method is able to address the challenges

associated with dense time-lapse phase contrast and HeLa data and it shows similar or improved tracking and mitosis detection performance when compared to those obtained by other relevant implementations that were reported in the literature.

V. CONCLUSIONS

In this paper we detailed the development of a novel algorithm that is able to automatically track the cells and detect mitosis in complex time-lapse phase contrast image sequences. The proposed tracking framework evaluates the local structure that encodes the neighbouring relationships between cells in adjacent frames of the sequence, where the tracking process does not require any prior knowledge regarding the cell morphology or migration patterns. Under-segmentation and mitosis detection were successfully dealt with by using a pattern recognition-based algorithm that is enforced by evaluating in a sequential manner the local structural information that is sampled in a Delaunay mesh representation. The proposed algorithm has been evaluated on several cellular datasets with various challenging conditions such as unstructured cellular motion, shape variation, intensity variation, cellular agglomeration and image noise. The overall tracking accuracy achieved by the proposed method is 86.10% where the accuracy in detecting mitosis is 90.12%.

APPENDIX - SUPPLEMENTARY MULTIMEDIA MATERIALS

Video sequences have been submitted as supplementary multimedia material to illustrate the tracking results obtained by the proposed method when applied to cell-specific datasets. The multimedia files can be accessed by visiting the following webpage:

<http://elm.eeng.dcu.ie/~cipa/videos/>

Please refer to the README file that provides full details in regard to the cellular data and the interpretation of the visual results. The size of the supplementary material is 169.9 MB.

ACKNOWLEDGMENT

We would like to thank Dr. András Czırók, Department of Anatomy and Cell Biology, University of Kansas Medical Centre for his valuable suggestions during the development stage of the cell tracking algorithm.

REFERENCES

- [1] F. Li, X. Zhou, J. Ma, and S. T. C. Wong, "Multiple nuclei tracking using integer programming for quantitative cancer cell cycle analysis," *IEEE Trans. Medical Imaging*, vol. 29, no. 1, pp. 96-105, Jan. 2010.
- [2] I. Adanja, O. Debeir, V. Megalizzi, R. Kiss, N. Warzee, and C. Decaestecker, "Automated tracking of unmarked cells migrating in three-dimensional matrices applied to anti-cancer drug screening," *Experimental Cell Research*, vol. 316, no. 2, pp. 181-193, Jan. 2010.
- [3] A. Tremel, A. Cai, N. Tirtaatmadja, B. D. Hughes, G.W. Stevens, K. A. Landman, and A. J. O'Connor, "Cell migration and proliferation during monolayer formation and wound healing," *Chemical Engineering Science*, vol. 64, no. 2, pp. 247-253, Jan. 2009.
- [4] O. Al-Kofahi, R. J. Radke, S. K. Goderie, Q. Shen, S. Temple, and B. Roysam, "Automated cell lineage construction: A rapid method analysis clonal development established with murine neural progenitor cells," *Cell Cycle*, vol. 5, no. 3, pp. 327-335, Feb. 2006.

- [5] O. Debeir, P. van Ham, R. Kiss, and C. Decaestecker, "Tracking of migrating cells under phase-contrast video microscopy with combined mean-shift processes," *IEEE Trans. Medical Imaging*, vol. 24, no. 6, pp. 697–711, Jun. 2005.
- [6] O. Debeir, I. Camby, R. Kiss, P. van Ham, and C. Decaestecker, "A model-based approach for automated in vitro cell tracking and chemotaxis analyses," *Cytometry Part A*, vol. 60, no. 1, pp. 29–40, Jul. 2004.
- [7] S. K. Nath, F. Bunyak, and K. Palaniappan, "Robust tracking of migrating cells using four-color level set segmentation," *Lecture Notes in Computer Science*, vol. 4179, pp. 920–932, 2006.
- [8] K. Thirusittampalam, M. J. Hossain, O. Ghita, and P. F. Whelan, "A novel framework for tracking in-vitro cells in time-lapse phase contrast data," in *Proc. British Machine Vision Conference*, UK, 2010, pp. 69.1–69.11.
- [9] M. A. Dewan, M. O. Ahmad, and M. N. S. Swamy, "Tracking biological cells in time-lapse microscopy: an adaptive technique combining motion and topological features," *IEEE Trans. Biomedical Engineering*, vol. 58, no. 6, pp. 1637–1647, Jun. 2011.
- [10] A. Genovesio, T. Liedl, V. Emiliani, W. J. Parak, M. C. Moisan, and J. C. Olivo-Marin, "Multiple particle tracking in 3D+t microscopy: method and application to the tracking of endocytosed quantum dots," *IEEE Trans. Image Processing*, vol. 15, no. 5, pp. 1062–1070, May 2006.
- [11] N. Ray, S. T. Acton, and K. Ley, "Tracking leukocytes in-vivo with shape and size constrained active contours," *IEEE Trans. Medical Imaging*, vol. 21, no. 10, pp. 1222–1234, Oct. 2002.
- [12] C. Zimmer, E. Labruyere, V. Meas-Yedid, N. Guillen, and J. C. Olivo-Marin, "Segmentation and tracking of migrating cells in videomicroscopy with parametric active contours: a tool for cell based drug testing," *IEEE Trans. Medical Imaging*, vol. 21, no. 10, pp. 1212–1221, Oct. 2002.
- [13] A. Sacan, H. Ferhatosmanoglu, and H. Coskun, "CellTrack: an open-source software for cell tracking and motility analysis," *Bioinformatics*, vol. 24, no. 14, pp. 1647–1649, May 2008.
- [14] D. P. Mukherjee, N. Ray, and S. T. Acton, "Level set analysis for leukocyte detection and tracking," *IEEE Trans. Image Processing*, vol. 13, no. 4, pp. 562 – 572, Apr. 2004.
- [15] A. Dufour, V. Shinin, S. Tajbakhsh, N. Guillén-Aghion, J. C. Olivo-Marin, and C. Zimmer, "Segmenting and tracking fluorescent cells in dynamic 3-D microscopy with coupled active surfaces," *IEEE Trans. Image Processing*, vol. 14, no. 9, pp. 1396–1410, Sep. 2005.
- [16] O. Dzyubachyk, W. A. van Cappellen, J. Essers, W. J. Niessen, and E. Meijering, "Advanced level-set-based cell tracking in time lapse fluorescence microscopy," *IEEE Trans. Medical Imaging*, vol. 29, no. 3, Mar. 2010.
- [17] X. Yang, H. Li, and X. Zhou, "Nuclei segmentation using marker-controlled watershed, tracking using mean-shift, and Kalman filter in time-lapse microscopy," *IEEE Tran. Circuits and Systems*, vol. 53, no. 11, pp. 2405–2414, Nov. 2006.
- [18] I. Smal, K. Draegestein, N. Galjart, W. Niessen, and E. Meijering, "Particle filtering for multiple object tracking in dynamic fluorescence microscopy images: application to microtubule growth analysis," *IEEE Trans. Medical Imaging*, vol. 27, no. 6, pp. 789–803, Jun. 2008.
- [19] S. Huh, D. F. E. Ker, R. Bise, M. Chen, and T. Kanade, "Automated mitosis detection of stem cell populations in phase-contrast microscopy images," *IEEE Trans. Medical Imaging*, vol. 30, no. 3, pp. 586–596, Mar. 2011.
- [20] X. Chen, X. Zhou, and S. T. Wong, "Automated segmentation, classification, and tracking of cancer cell nuclei in time-lapse microscopy," *IEEE Trans. Biomedical Engineering*, vol. 53, no. 4, pp. 762–766, Mar. 2006.
- [21] X. Song, F. Yamamoto, M. Lguchi, and Y. Murai, "A new tracking algorithm of PIV and removal of spurious vectors using Delaunay tessellation," *Experiments in Fluids*, vol. 26, no. 4, pp. 371–380, Mar. 1999.
- [22] P. Soille, *Morphological Image Analysis: Principles and Applications*, New York: Springer-Verlag, 2003.
- [23] N. Otsu, "A threshold selection method from gray-level histogram," *IEEE Trans. Systems, Man, and Cybernetics*, vol. 9, no. 1, pp. 62–66, Jan. 1979.
- [24] M. de Berg, O. Cheong, M. van Kreveld, and M. Overmars, *Computational Geometry: Algorithms and Applications*, Heidelberg: Springer-Verlag, 2008, pp. 198–218.
- [25] D. Tsai and C. Lin, "Fast normalized cross correlation for defect detection," *Pattern Recognition Letters*, vol. 24, no. 15, pp. 2625–2631, Nov. 2003.
- [26] T. Kanade, Z. Yin, R. Bise, S. Huh, S. Eom, M.F. Sandbothe, and M. Chen, "Cell image analysis: Algorithms, system and applications," in *Proc. IEEE Workshop on Applications of Computer Vision*, Kona, 2011, pp. 374–381.
- [27] S. Huh, S. Eom, R. Bise, Z. Yin, and T. Kanade, "Mitosis detection for stem cell tracking in phase-contrast microscopy images," in *Proc. IEEE International Symposium on Biomedical Imaging: From Nano to Macro*, Chicago, 2011, pp. 2121 – 2127.
- [28] F. Li, X. Zhou, J. Ma and S.T.C. Wong, "A Novel Cell Segmentation Method and Cell Phase Identification Using Markov Model" *IEEE Trans. Information Technology in Biomedicine*, vol. 13, no. 2, pp. 152–157, Mar. 2009.
- [29] Z. Yin, K. Li, T. Kanade, and M. Chen, "Understanding the optics to aid microscopy image segmentation," in *Proc. Int. Conf. on Medical Image Computing and Computer-Assisted Intervention*, Beijing, China, 2010, vol. 6361, pp. 209–217.
- [30] C. Tang, L. Ma, and D. Xu, "Topological constraint in high-density cells' tracking of image sequences," *Advances in Experimental Medicine and Biology*, vol. 696, pp. 255–262, 2011.
- [31] L. Zhang, H. Xiong, K. Zhang, and X. Zhou, "Graph theory application in cell nucleus segmentation, tracking and identification," in *Proc IEEE Int. Symposium on Bioinformatics and Bioengineering*, Boston, USA, 2007, pp. 226–232.

Ketheesan Thirusittampalam is currently pursuing his PhD degree in Biomedical Engineering within the Centre for Image Processing and Analysis (CIPA), Dublin City University (DCU), Ireland. His research work is focused on the segmentation and tracking of in-vitro cells in microscopy images.

M. Julius Hossain received his B.S. and M.S. degrees in Computer Science from University of Dhaka, Bangladesh in 2000 and 2002, respectively. He received his Ph.D. degree in Computer Engineering from Kyung Hee University, South Korea in 2008. He has been working as a faculty member in the Department of Computer Science and Engineering, University of Dhaka, Bangladesh since 2003. Currently, he is working as a Postdoctoral Research Fellow in the Centre for Image Processing and Analysis, Dublin City University, Ireland. His research interest includes motion detection, automated video surveillance and tracking cellular and sub-cellular structures in microscopy images.

Ovidiu Ghita received the BE and ME degrees in Electrical Engineering from Transilvania University Brasov, Romania and the Ph.D. degree from Dublin City University, Ireland. From 1994 to 1996 he was an Assistant Lecturer in the Department of Electrical Engineering at Transilvania University. Since then he has been a member of the Vision Systems Group at Dublin City University (DCU) and currently he holds a position of DCU-Research Fellow. Dr. Ghita has authored and co-authored over 90 peer-reviewed research papers in areas of instrumentation, range acquisition, machine vision, texture analysis and medical imaging.

Paul F. Whelan (S'84-M'85-SM'01) received his B.Eng. (Hons) degree from NIHED, M.Eng. from the University of Limerick, and his Ph.D. (Computer Vision) from the University of Wales, Cardiff, UK. During the period 1985–1990 he was employed by Industrial and Scientific Imaging Ltd and later Westinghouse (WESL), where he was involved in the research and development of high-speed computer vision systems. He was appointed to the School of Electronic Engineering, Dublin City University (DCU) in 1990 and is currently Professor of Computer Vision (Personal Chair). Prof. Whelan founded the Vision Systems Group in 1990 and the Centre for Image Processing & Analysis in 2006 and currently serves as its director.

As well as publishing over 150 peer reviewed papers, Prof. Whelan has co-authored 2 monographs and co-edited 3 books. His research interests include image segmentation, and its associated quantitative analysis with applications in computer/machine vision and medical imaging. He is a Senior Member of the IEEE, a Chartered Engineer, member of the IAPR and a Fellow of the IET. He served as a member of the governing board (1998–2007) of the *International Association for Pattern Recognition* (IAPR), a member of the *International Federation of Classification Societies* (IFCS) council and President (1998–2007) of the *Irish Pattern Recognition and Classification Society* (IPRCS). Prof. Whelan is a HEA-PRTL (RINCE, NBIP) and Enterprise Ireland funded principal investigator.